

BED MOTION UNDER WAVES: PLUG AND SHEET FLOW OBSERVATIONS

Hervé Michallet¹, Eric Barthélemy¹, Arnout Lammens¹, Giulia Marin¹ and Gérard Vaudelin¹

Abstract

Experiments were designed to address the role of horizontal pressure gradients on bed dynamics for shoaling, breaking, surf and swash waves. A small-scale laboratory flume with low density sediment is used. The flow in the bottom boundary layer and sediment bed motion is tracked by video measurements. Occurrence of plug flows is evidenced. We also question the role of the vertical pressure gradients on bed destabilization, and the dubious relevance of acoustic measurements to track deep layers of moving sediment. The chosen experimental set-up is favoring the occurrence of the plug flow regime, scaling arguments nevertheless suggest that plug flow is likely to occur in natural coastal zones.

Key words: hydrodynamics, sediment transport, morphodynamics.

1. Introduction

Identified for several decades (e.g. Madsen, 1974), horizontal pressure gradient effects on bed destabilization have gain further interest in recent years for improving sediment transport computation in the nearshore (e.g. Lanckriet and Puleo 2015, Cheng et al., 2017). Sleath (1999) defined the transport regime induced by horizontal pressure gradients, leading a whole layer of sediment to move as a block, and called it ‘plug flow’. Defining a Sleath number as

$$S = \frac{\partial p / \partial x}{(\rho_s - \rho)g} \quad (1)$$

where ρ and ρ_s are the water and sediment densities, p the pressure, x the horizontal coordinate and g the gravitational acceleration, it can be shown that bed failure occurs if $|S| \geq K_f C$, with K_f (≈ 0.6) the internal friction angle and C (≈ 0.5) the sediment concentration. The plug flow regime is in marked contrast with the sheet flow regime. The latter is produced by large bed shear stresses and characterized by velocity and concentration gradients in a layer of moving sediments of about 5 to 15 grain size thickness. Recent laboratory experiments have shown evidence of both regimes in the surf zone (Berni et al., 2013, 2017). Here we further study the bed dynamics for shoaling, breaking and swash waves, with increased resolution by video recording. We also question the role of the vertical pressure gradients on bed destabilization, and the relevance of acoustic measurements to track deep layers of moving sediment and especially in very shallow water.

¹Univ. Grenoble Alpes, LEGI – UMR 5519, CS40700, 38041 Grenoble cedex 9, France, herve.michallet@legi.cnrs.fr

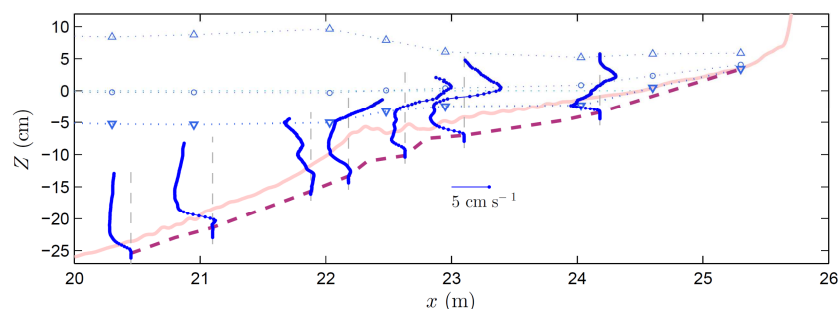


Figure 1. Vertical profiles of the mean horizontal velocity (blue dotted line) along the final beach profile once waves have ceased (thick solid line) and lowest elevation of the moving bed during the whole experiment (thick dashed line). Upward-pointing triangles, circles and downward-pointing triangles represent maximum, mean and minimum water elevation, respectively. $Z = 0$ is the water level at rest, $x = 0$ is at the wave-maker.

2. Experimental set-up

Experiments were performed in the LEGI wave flume (36 m long, 0.55 m wide) filled with water at a depth of 55.3 cm and a beach of light-weight sediment ($\rho_s = 1.18 \text{ kg L}^{-1}$, with median diameter $d_{50} = 0.64 \text{ mm}$). The sediment choice is meant to reproduce bed load and suspension transports through fulfilling both Shields and Rouse scaling laws, when considering a length scale of 1/10 relatively to natural beaches (Grasso et al., 2009, 2011a, 2011b). More recent experiments by Berni et al. (2013, 2017) enlightened the physics of the flow boundary layer over the moving bed, emphasizing the pressure gradients effects on bed erosion.

A piston-type wave maker produced a pair of bichromatic wave packets (the amplitude of both components is 3 cm, their frequencies are $f_1 = 0.5515 \text{ Hz}$ and $f_2 = 0.625 \text{ Hz}$, leading to an exact repetition of a 27.2 s wave series made of two groups). The beach was let to evolve so as to reach a quasi-equilibrium state of average slope 1:20 and with a nearshore bar where waves break at $x = 22.2 \text{ m}$. These conditions were shown to produce beach profiles oscillating slightly around a mean profile at very large time scales (of the order of 1000 s, see Rocha, 2016).

The whole experiment lasted 5 hours. During the experiment, a high-speed video camera was moved at 11 different cross-shore positions so as to record, through the glass wall, 42 s of the wave series (three wave packets) in the shoaling, breaking, surf and swash zones. Each field of view was 30 cm long and 20 cm high. The flow was video recorded at 160 frames per second. Velocity fields with a spatial resolution of 1 mm are obtained through correlation methods.

In addition, twelve capacitive wave gages were installed at various positions to monitor water elevation along the beach profile. Three pore pressure sensors, installed at and within the bed of sediment, were located slightly off-shore the break point at $x = 21.3 \text{ m}$.

A synthetic overview of the mean flow generated by the wave transformation and breaking is presented in Figure 1. The wave action reworked several centimeters of the bed, with the deepest erosion occurring in the breaking zone ($x \sim 22.3 \text{ m}$). A limited amount of the sediment is set into motion during the full wave sequence, as will be seen in the next section. Nevertheless, mean velocities are recorded well below the bed level at rest. These are mainly off-shore directed, except very close to the non-moving bed where they can be oriented onshore (see the profiles at $x \sim 21.1 \text{ m}$ $x \sim 22.2 \text{ m}$ for instance). Local maxima of the off-shore oriented mean velocity approximately correspond to the minimum of the wave trough level. For the three most onshore profiles, local maxima of the onshore directed mean velocity correspond to the mean water level.

3. Results

3.1. Plug flow observation

Examples of time stacks extracted from the velocity fields are shown in Figures 2, 3 and 4 corresponding to the shoaling, breaking and swash zones, respectively. For evaluating the potential for plug flow formation, the Sleath number S is computed with (1) and $\partial p/\partial x = -\rho \partial u_\infty/\partial t$, where u_∞ is the free stream velocity recorded at $z = 1$ cm above the initial bed elevation. Berni et al. (2017) indeed confirmed that the flow acceleration is a good proxy for horizontal pressure gradients in the bed.

In the shoaling zone (Figure 2), horizontal velocities are vertically uniform in most of the water column. A slight phase lead can be seen when approaching the bed. The Sleath number estimate indicates that the plug flow threshold $S = \pm 0.3$ is reached for the largest waves. The onset under the steep wave fronts corresponds to upward directed vertical velocities at the bed. Downward vertical velocities under wave troughs are weak close to the bed, further confirming that a few mm thick moving layer of sediment is set on at flow reversal after the wave crest.

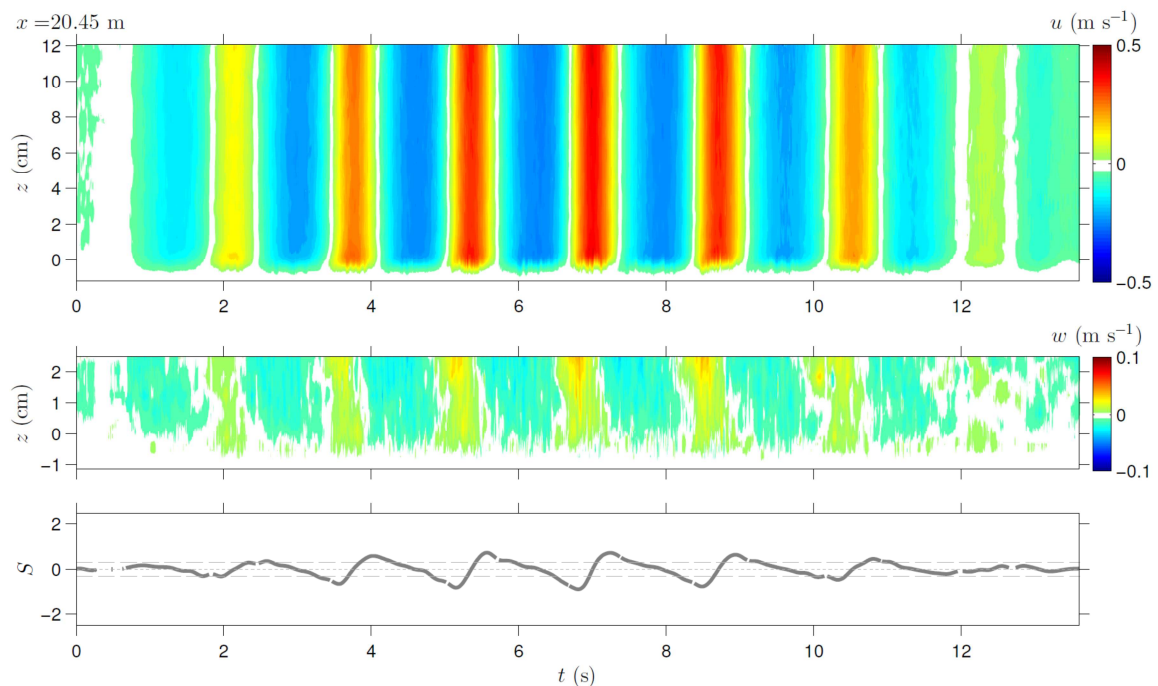


Figure 2. Time series of vertical profiles of horizontal (top) and vertical (middle) velocities in the shoaling zone.

Bottom panel: Sleath number computed from the horizontal acceleration $\partial u_\infty/\partial t$, where u_∞ is the free stream velocity recorded at $z = 1$ cm (horizontal dashed lines are threshold values for plug flow: $S = \pm 0.3$), $z = 0$ is the initial bed level at rest.

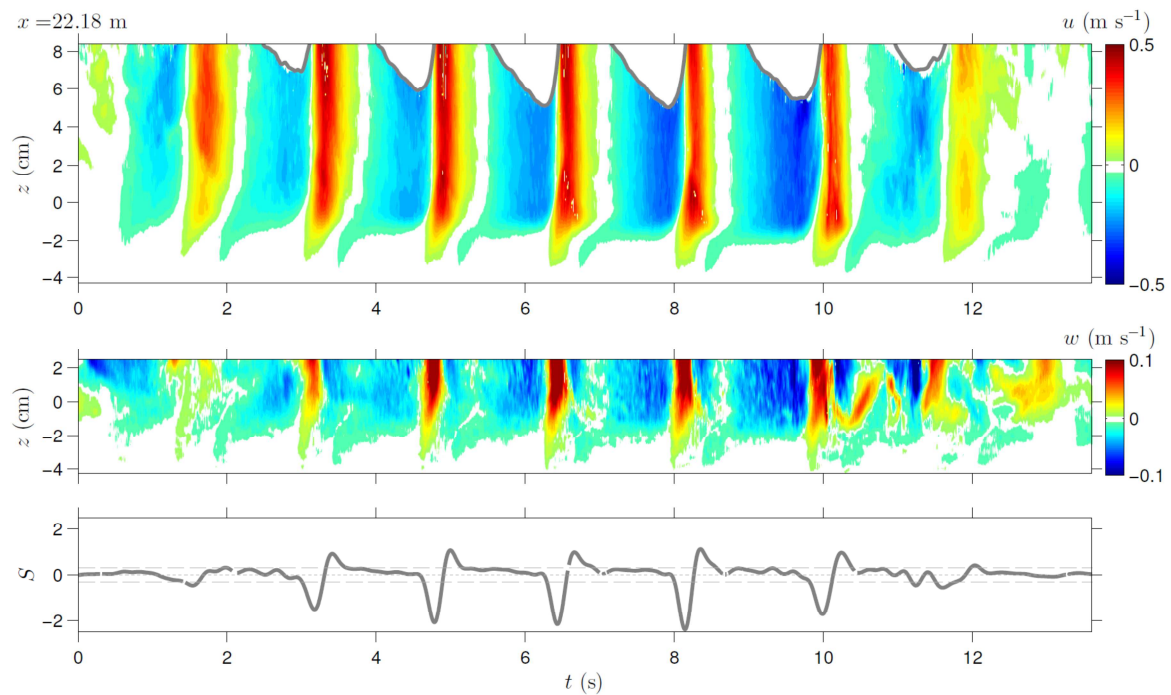


Figure 3. Same as in Figure 2, for the breaking zone. The thick line in the top panel is the free surface elevation recorded with the capacitive wave gage.

In the breaking zone (Figure 3), the plug flow dynamics is more obvious. The wave fronts are very steep and very large values of S can be obtained. Once reached the threshold value of -0.3 , vertical velocities oriented upwards are recorded deep into the bed, while horizontal velocities are roughly uniform over that sediment layer of a few centimeters thick. Under the wave crests, as the free stream horizontal velocity is maximum, the plug flow becomes thinner and turns into a sheet flow as the velocity gradient at the bed increases. Just after the wave crest, the flow acceleration becomes largely negative and a transient plug flow directed off-shore is observed too.

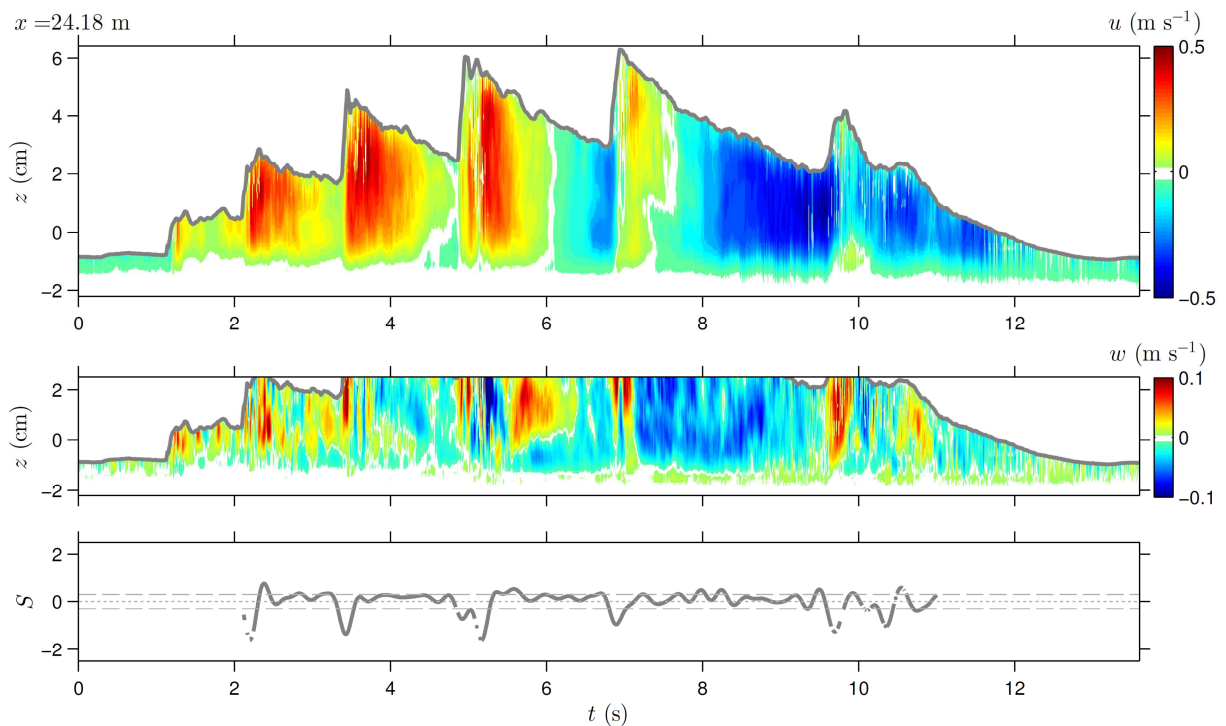


Figure 4. Same as in Figure 3, for the swash zone.

In the swash zone (Figure 4), large accelerations only occur at the short wave fronts and for a more limited duration compared to the previous case. They nevertheless still induce onshore plug flow.

3.2. Vertical pressure gradients and shear stress estimate

Figure 5 provides in more detail an example of pressure and velocity measurements just prior to wave breaking (at $x = 21.3$ m). The phase lead of the horizontal velocity in the bottom boundary layer is clearly seen. A bed destabilization of about 2 cm deep (about 30 grain sizes) is observed ahead of each wave front. This corresponds to a plug flow, as confirmed by the estimate of the Sleath number exceeding the threshold value of 0.3. Slightly ahead of the plug initiation, upward vertical velocities (third panel) are recorded in phase with vertical pressure differences (bottom panel) that overcome the soil weight column so to reach a threshold for liquefaction (see e.g. Scholtès et al., 2015). This emphasizes that wave induced vertical pressure gradients play a role in bed destabilization. Most of the wave cycle is characterized by mobile layers of about 10 grain sizes thick, corresponding to relatively large shear stress values at $z = 0$. These are clearly characteristic of the sheet flow regime. Of note, the measured granular shear stress is relatively weak in the mobile layer (fifth panel). This underlines that pressure gradient effects are crucial for sediment transport in our physical model.

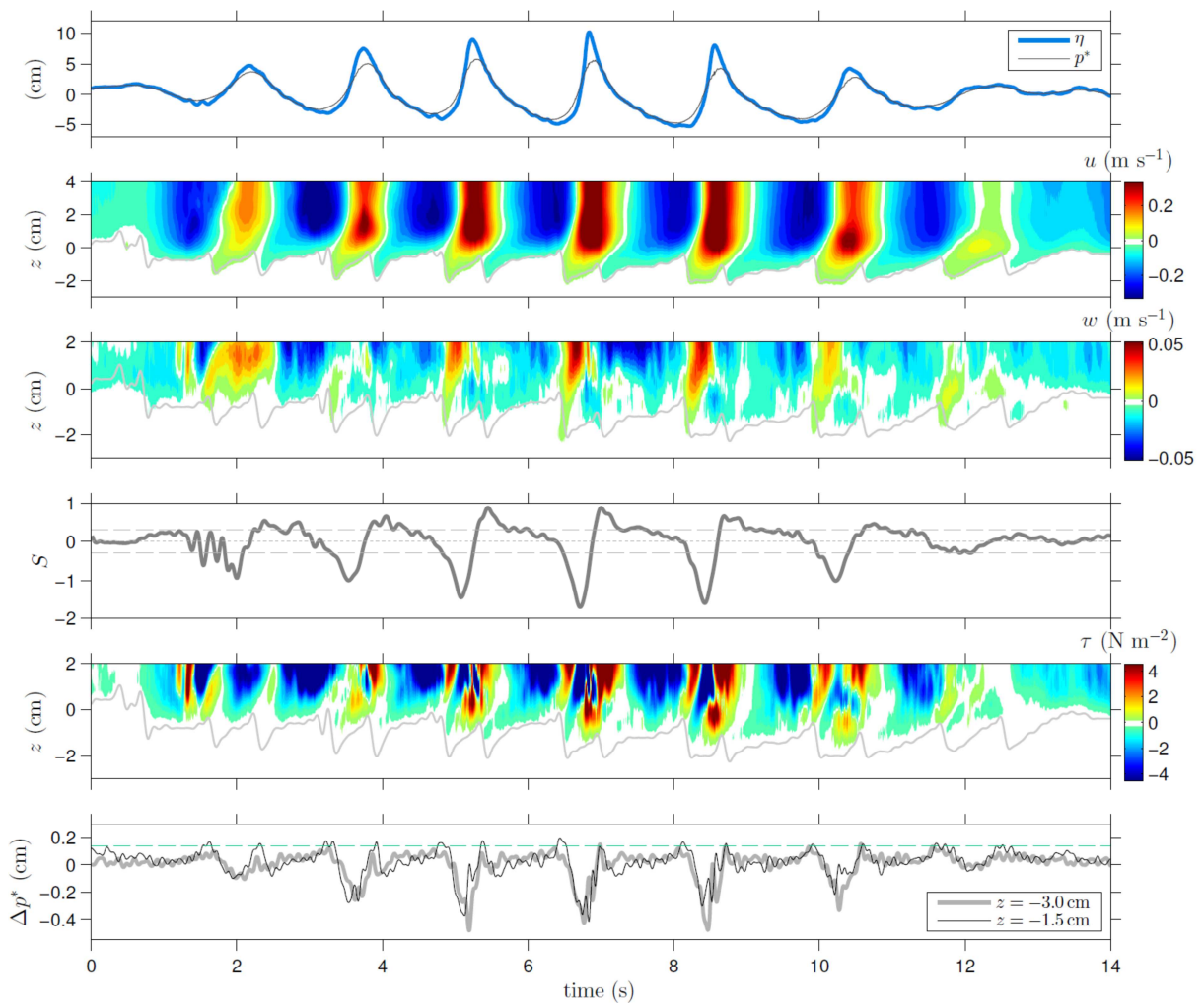


Figure 5. Selected time series of, from top to bottom: free surface elevation η and excess pressure at the bed p^* , horizontal velocity u (the gray solid line is the boundary of the non-moving bed determined for a velocity norm threshold of 5 mm s^{-1}), vertical velocity w , Sleath number S (horizontal dashed lines are threshold values for plug flow: $S = \pm 0.3$), shear stress $\tau = -\rho uw$, excess pore pressure vertical difference between the bed at rest ($z = 0$) and $z = -1.5$ cm (black) and between $z = -1.5$ cm and $z = -3$ cm (gray) with dashed line representing threshold value for liquefaction. The water depth at the measurement location ($x = 21.31$ m) is 18 cm.

3.3. Velocity field example

An example of the spatial onset of the plug flow is shown in Figure 6. As velocities are oriented off-shore in the water column, a two centimeters thick bed layer is flowing onshore (top left). This corresponds to upward vertical velocities characteristic of bed erosion (top right). Shear layers develop at the bed and below the plug as indicated by the representation of the velocity curl (bottom left). In the bed, the velocity divergence is an estimate of the change in porosity. The bottom right panel in Figure 6 seemingly indicates bed dilation ($du/dx + dw/dz > 0$) inside the plug and compaction ($du/dx + dw/dz < 0$) just above it.

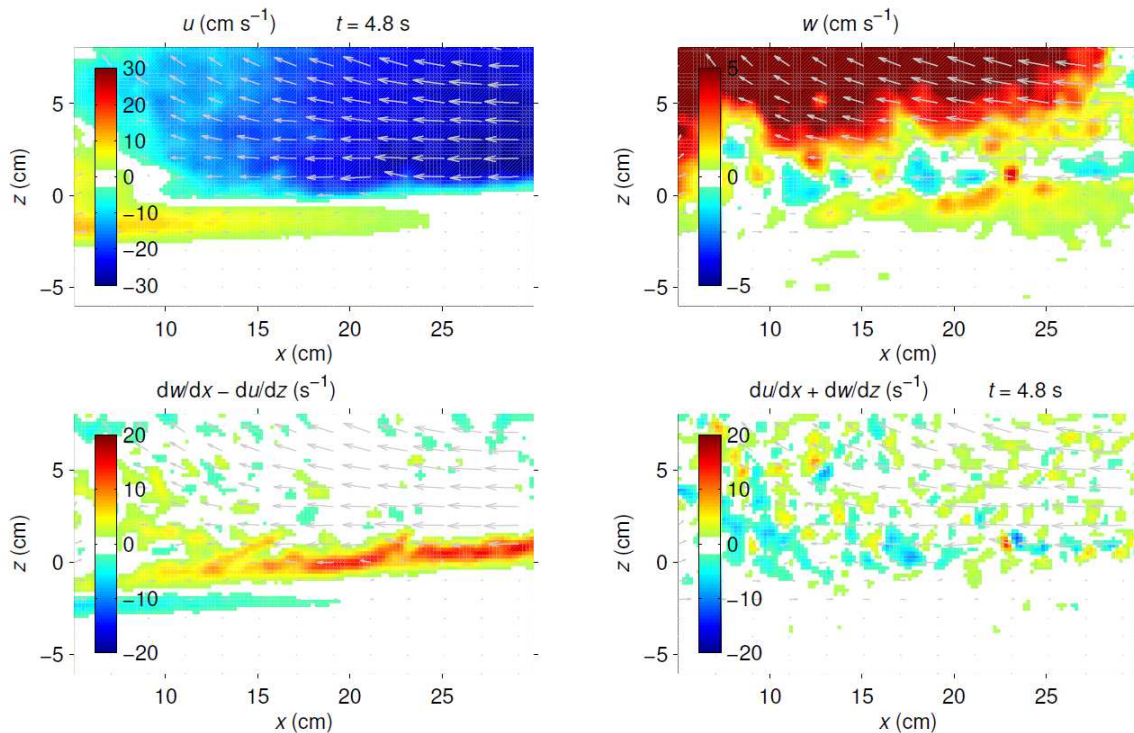


Figure 6. Horizontal (top left) and vertical (top right) velocity fields, curl (bottom left) and divergence (bottom right). The time corresponds to $t = 4.8$ s of the time series in Figure 5. Here x is the horizontal distance in the field of view, $x = 25$ cm corresponds to the position relatively to the wave-maker $x = 21.31$ m.

3.4. Comparison with acoustic measurements

Acoustic sensors obviously cannot operate in very shallow water such as the swash zone for which video measurements are shown in Figure 4. It is worth to note that, while operational in the surf zone with mobile layers of sediment of less than 10 grain size thick (see Berni et al., 2017), acoustic sensors fail in most of the breaking zone due to acoustic signal attenuation by sediment suspension. An example is shown in Figure 7. Compared to the PIV measurements shown in Figure 5, the ADV misses the boundary layer phase lead and thus cannot capture the plug flow. The velocity estimate is apparently not reliable below the elevation where the acoustic signal is reaching its maximum value (shown in the bottom panel of Figure 7).

Figure 8 further shows that PIV and ADV measurements agree fairly well at about 1 cm above the bed but do not match when entering in the moving bed ($z = 0$). At $z = 1$ cm, discrepancies are seen at the beginning of the time series (at $t \sim 2$ s) at the time of very low acoustic signal amplitude (as shown in the bottom panel of Figure 7). This is due to high sediment concentration induced by a turbidity current flowing down the beach slope at that stage of the wave series (see Rocha, 2016). For the rest of the signal, both vertical velocity measures are similar (second panel in Figure 8). This indicates that the acoustic wave trains backscatters on the same tracers and sediment mixture than the one used for correlating images by PIV. Here it is suspected that both techniques might lead to similar bias accounting for the sediment settling velocity.

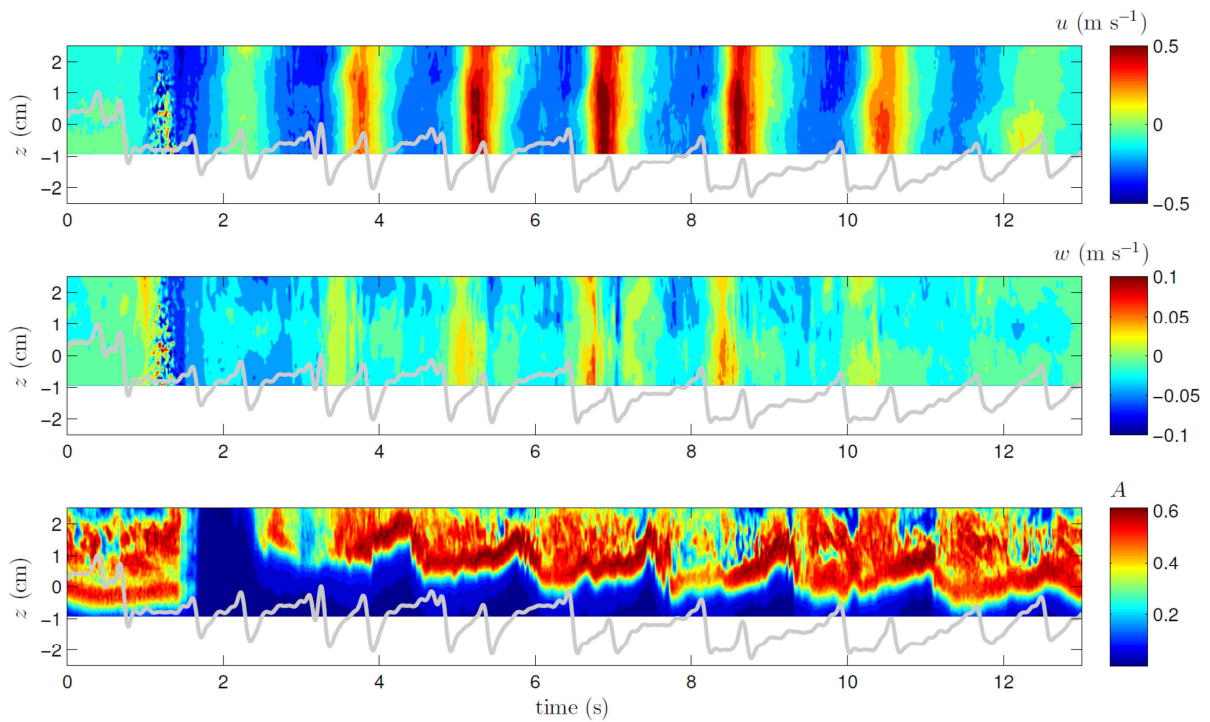


Figure 7. Horizontal (top) and vertical (middle) velocities, and dimensionless acoustic signal amplitude, recorded with the ADV. The measurements are collocated and synchronized with the PIV measurements plotted in Figure 5. The grey line is the non-moving bed interface deduced from the PIV.

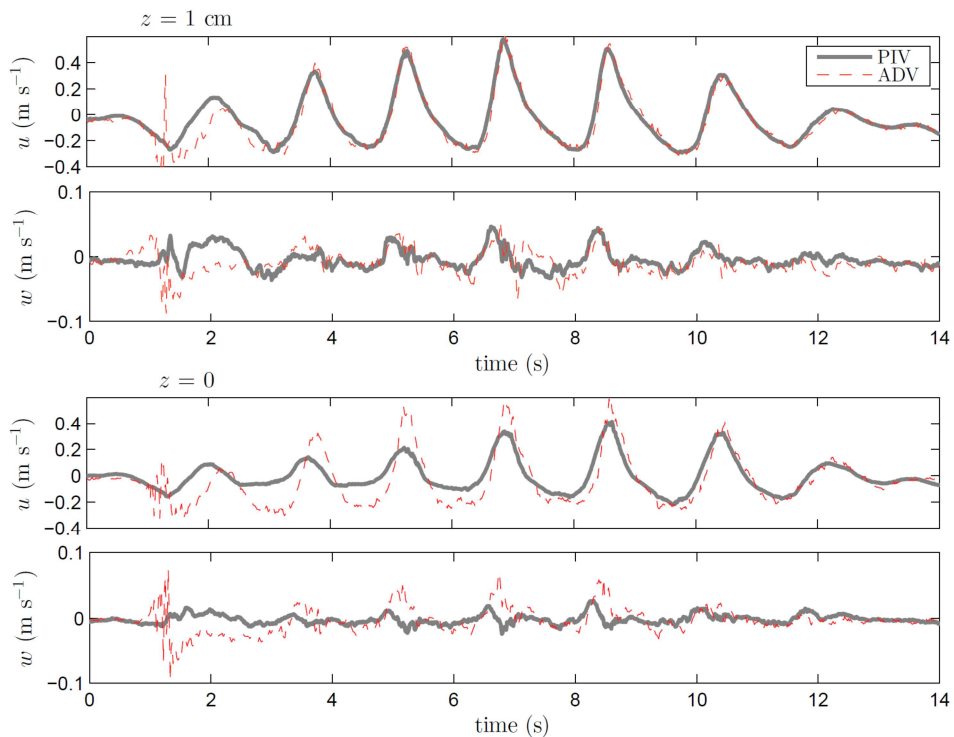


Figure 8. Comparison between PIV (thick solid line) and ADV (dashed) horizontal (u) and vertical (w) velocity measurements at 1 cm above the bed (two upper panels) and in the moving bed (two bottom panels).

In marked contrast, large discrepancies are seen for the measurements in the moving bed. The PIV measurements are consistent with the erosion depths that can be deduced from the pressure measurements and consistent with the phase leading boundary layer theory. It is troublesome that the ADV technique provides velocity signals at $z = 0$ that mimic the real velocities measured 1 cm above. It suggests that one should carefully discard the fake velocity signals from elevations where the acoustic amplitude is weak.

4. Discussion and conclusions

Experiments have been presented to study sediment transport in shoaling, breaking, surf and swash zones. A synthesis is presented in Figure 9. The short waves break at $x \sim 22$ m and low frequencies dominate on-shore $x \sim 23$ m. Wave skewness and asymmetry are considered of major importance in triggering sediment transport in the coastal zone (e.g. Grasso et al., 2011, Berni et al., 2011). We note here that large asymmetry values are observed in the outer surf zone ($22 < x < 23$ m). They are the signature of very steep wave fronts and unsurprisingly correspond to large values of the maximum Sleath number, indicating on-shore directed intense plug flow. Yet less intense, off-shore directed plug flow is observed too.

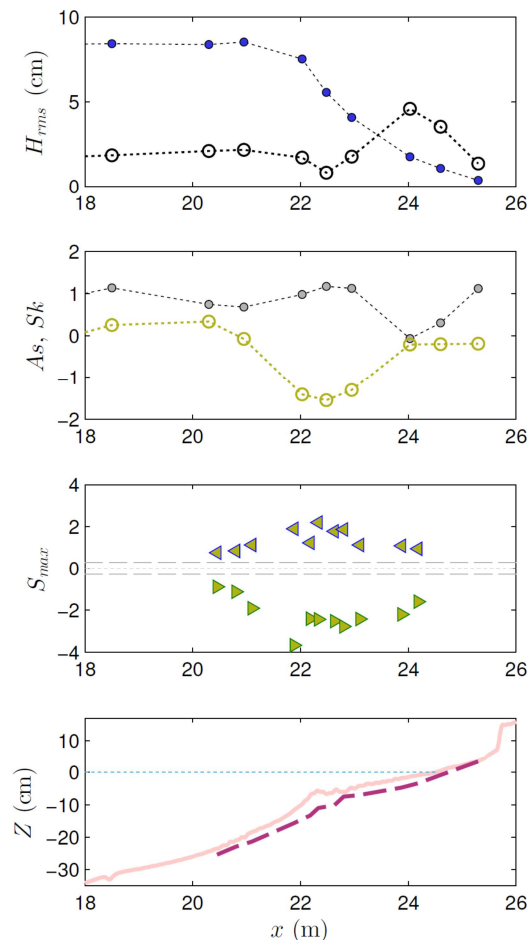


Figure 9. Top: short wave (dots) and long wave (circles) wave heights. Second panel: wave skewness (dots) and asymmetry (circles). Third panel: maximum in Sleath number magnitude recorded during the wave series, favoring onshore transport (right-pointing triangles) and favoring off-shore transport (left-pointing triangles), with horizontal dashed lines indicating threshold values for plug flow ($S = \pm 0.3$).

Bottom panel: beach profile once waves have ceased (solid line) and maximum elevation of the non-moving bed during the wave sequence (thick dashed line), $Z = 0$ is the water level at rest.

The choice of low density sediment to fulfill Shields and Rouse scaling requirements in a laboratory flume (length scale of 1/10 relatively to typical field conditions) comes with side effects. Low density sediment is more subject to pressure gradient effects. Most importantly, the relative horizontal pressure gradient (or Sleath number S) is found to be roughly 8 times larger than for waves in the field, the wave shape and flow acceleration scaling perfectly through the Froude number. This leads to favor plug flow transport in our laboratory experiment. It is shown to be a dominant mechanism, leading to deep bed erosion under each steep wave front.

The experiments confirm that plug flow sediment transport occurs for $S > 0.3$. Once scaled to natural environments, our measurements suggest that this regime is very likely to occur in the breaking zone. Besides, horizontal pressure gradient effects associated to strong flow accelerations under steep wave fronts are not to be neglected in the coastal zone. Potentially of the same order of magnitude as bed shear stress effects, pressure gradients certainly largely contribute to onshore sediment transport. This was formerly pointed out by Madsen (1974), further shown by Sleath (e.g. 1999), investigated for field condition by Foster et al. (2006), and more recently in large scale laboratory experiments by Anderson et al. (2017).

Acknowledgements

The support of F. Bonnel from GINP - IRIS unit on video capturing has been greatly appreciated. The PIV software UVMAT is developed by J. Sommeria, whose help is gratefully acknowledged.

References

- Anderson, D., Cox, D., Mieras, R., Puleo, J.A. and Hsu, T.-J., 2017. Observations of wave-induced pore pressure gradients and bed level response on a surf zone sandbar. Submitted to *J. Geophys. Res. Oceans*.
- Berni, C., Barthélemy, E. and Michallet, H., 2013. Surf zone cross-shore boundary layer velocity asymmetry and skewness: an experimental study on a mobile bed. *J. Geophys. Res. Oceans*, 118: 2188–2200.
- Berni, C., Michallet, H. and Barthélemy, E., 2017. Effects of horizontal pressure gradients on bed destabilization under waves. *J. Fluid Mech.* 812: 721–751.
- Cheng, Z., Hsu, T.-J. and Calantoni, J., 2017. SedFoam: A multi-dimensional Eulerian two-phase model for sediment transport and its application to momentary bed failure. *Coastal Engng.*, 119: 32–50.
- Foster, D.L., Bowen, A.J., Holman, R. A. and Natto, P., 2006. Field evidence of pressure gradient induced incipient motion. *J. Geophys. Res.*, 111: C05004.
- Grasso, F., Michallet, H., Barthélemy, E. and Certain, R. 2009. Physical modeling of intermediate cross-shore beach morphology: transients and equilibrium states. *J. Geophys. Res.*, 114: C09001.
- Grasso, F., Michallet, H., and Barthélemy, E., 2011. Experimental simulation of shoreface nourishments under storm events: A morphological, hydrodynamic, and sediment grain size analysis. *Coastal Engng.*, 58(2): 184–193.
- Grasso, F., Michallet, H., and Barthélemy, E., 2011. Sediment transport associated with morphological beach changes forced by irregular asymmetric-skewed waves. *J. Geophys. Res.*, 116: C03020.
- Lanckriet, T. and Puleo, J.A., 2015. A semianalytical model for sheet flow layer thickness with application to the swash zone. *J. Geophys. Res.*, 120 (2): 1333–1352.
- Madsen, O.S. 1974 Stability of a sand bed under breaking waves. In *Proc. 14th Int. Conf. Coastal Engng*, 776–794.
- Rocha, M.V.L.M., 2016. *Observation and modelling of wave nonlinearities and infragravity waves in the nearshore*, PhD thesis Univ. Aveiro, Portugal and UGA, France.
- Scholtès, L., Chareyre, B., Michallet, H., Catalano, E. and Marzougui, D., 2015. Modeling wave-induced pore pressure and effective stress in a granular seabed. *Continuum Mech. Thermodyn.*, 27: 305–323.
- Sleath, J.F.A., 1999. Conditions for plug formation in oscillatory flow. *Cont. Shelf Res.*, 19 (13): 1643–1664.